Ohara Noriaki (Orcid ID: 0000-0002-7829-0779)
He Siwei (Orcid ID: 0000-0003-2432-3843)
Parsekian Andrew D (Orcid ID: 0000-0001-5072-9818)



# Spatial Snowdrift Modeling for an Open Natural Terrain using a Physically-based Linear Particle Distribution Equation

Noriaki Ohara[1], Siwei He[2, 3], Andrew D. Parsekian[1,4], Benjamin M. Jones[5], Rodrigo C. Rangel[4], Ian O. Nichols[6], Kenneth M. Hinkel[6]

[1]Department of Civil and Architectural Engineering, University of Wyoming, Laramie, WY, 82071, USA

[2] Cooperative Institute for Research in Environmental Sciences, University of Colorado, Boulder, CO, 80309, USA

[3] NOAA Global Systems Laboratory, Boulder, CO, 80305, USA

[4]Department of Geology and Geophysics, University of Wyoming, Laramie, WY 82071, USA

[5]Institute of Northern Engineering, University of Alaska Fairbanks, Fairbanks, AK 99775, USA

[6]Department of Geological and Mining Engineering and Sciences, Michigan Technological University, Houghton, MI 49931, USA

**Corresponding Author:** Noriaki Ohara

Civil and Architectural Engineering, University of Wyoming

1000 E. University Avenue, Laramie, Wyoming 82071

Phone:+1(307)343-2670; nohara1@uwyo.edu

This is the author manuscript accepted for publication and has undergone full peer review but has not been through the copyediting, typesetting, pagination and proofreading process, which may lead to differences between this version and the Version of Record. Please cite this article as doi: 10.1002/hyp.14468

**ABSTRACT**

Snowdrift, which results from deposition of wind transported snow, has been primarily estimated empirically rather than using physically-based modeling since the snow redistribution process is extremely complex. This study demonstrates a practical predictive model for snow redistribution based on the Linear Particle Distribution (LPD) equation, which consists of snow surface diffusion, snow surface advection, and snow surface erosion components. Here, we focus on numerical model development and implementation for two-dimensional natural terrains at meter-scale resolutions with and without perforated snow fences, which has been difficult to model in a two-dimensional field. First, a selected numerical scheme was implemented in the Snow Movement Over Open Terrain for Hydrology (SMOOTH) model platform and tested by the exact solutions under a few well-defined boundary conditions. Then, to simulate snowdrifts around the snow detention structures in the middle of the computational domain, an equivalent solid snow fence concept was introduced and tested. The model was applied to several terrains in the Laramie Range, Wyoming, and at two sites on the North Slope of Alaska, where wind-induced snow redistribution plays a major role. Data from Airborne Light Detection and Ranging (LiDAR), Ground Penetrating Radar (GPR), and Unmanned Aerial Vehicle (UAV) photogrammetry were used to calibrate and validate the model. The numerical snow redistribution model effectively reproduces the observed snowdrift distributions when snow densification and snowmelt effects were minimal. The model applications illustrated that the diffusion effect generally dominated snow redistribution with limited contributions of advection and erosion effects for abrupt terrain transition and perforated object, respectively.

## 1. Introduction

Wind redistribution of snow including snowdrifting around an object or abrupt terrain transition is important for the ecosystem in windswept, open areas in temperate and high-latitudes and altitudes. For example, the near surface ground temperature in Arctic polygonal tundra landscapes is sensitive to the redistributed snow depth that serves as an insulator (e.g. Bisht et al., 2018) for the underlying permafrost. However, the prediction of snow patterns around objects such as vegetation and buildings is not straightforward. Snowdrift is affected by numerous factors including, but not limited to, wind field, local turbulence, surface roughness, atmospheric boundary layer thickness, particle Reynolds number, snow particle size distribution, particle shape, density of snow particles in the air, and snow surface cohesion (e.g. Mott et al., 2016). Therefore, many coarse-scale land surface process models have ignored the effect of wind-snow redistribution because of limited understanding of the multiple factors that influence it. For estimation of snowdrifts around snow fences and for roof top snow load, for example, the empirical drift patterns developed from numerous field-observed and experimental profiles are typically used (e.g. Tabler, 2003; O'Rourke, 2010). However, further characterization of snow redistribution seems to be possible because there is a similarity among snowdrift patterns depending on the object type, local wind field, and antecedent weather conditions (e.g. Tabler, 1975).

One method to characterize snow distribution uses self-similarity theory, where snow thickness is represented as a fractal across a range of linear scales using various snow distribution data (Cline et al, 1998; Blöschl, 1999; Kuchment and Gelfan, 2001; Deems et al. 2006; Trujillo et al. 2007; Trujillo et al. 2009; Dadic et al., 2010; Grünewald et al., 2010; Mott et al., 2011). Recently, Moon et al. (2019) analyzed correlation structure in snow depth distribution

on sea ice using Multifractal Detrended Fluctuation Analysis (MF-DFA). They found an effective correlation structure within a 60 m grid while the structure became unclear on a larger scale. He et al. (2019) reached the same conclusion independently from LiDAR-derived snow depth over wind swept areas of the Rocky Mountains. The sharp decay in spatial correlation of snow depth implies that the pure statistical model insufficiently represents the sub-grid variability of snow at greater than 60 m grid resolution. However, it may be noteworthy that the combination of statistical characteristics with physically-based modeling was possible, for example, using the Fokker-Planck-Kolmogorov equation (FPE) that describes the evolving probability density function (PDF) of snow depth (He and Ohara, 2019).

Wind tunnel and water flume experiments have been considered effective to study snowdrifts around buildings based on the similarity between snow and other stable particles, such as high-density silica sand (Kind 1976, 1986; Iversen 1980; Kind and Murray, 1982; Anno, 1984; Oikawa et al., 2007) despite differences in particle material (Aksamit et al., 2016). Anno (1984) analyzed the snowdrift profiles around a perforated snow fence using a wind tunnel and clay particles. O'Rourke et al. (2004) used water channel experiments to characterize snow patterns and snow mass transport rates on gabled roofs, flat roofs, and stepped flat roofs. Zhang et al. (2010) studied the particle volume concentration distribution around the perforated snow fence using a wind tunnel. Wang et al. (2014) used an open circuit wind tunnel to examine the relationship of mass transport rate and particle deposition patterns around three dimensional stepped flat roofs. In such a well-defined flow domain, a Computational Fluid Dynamics (CFD) model is an effective tool to describe particle distribution. Uematsu (1991) performed snowdrift modeling around a solid snow fence using a CFD model. Tominaga et al., (1999) presented a CFD technique, the Launder-Kato-type k-ε model, for the prediction of snowdrift thickness

around a nine-story apartment building under construction. Beyers et al. (2004) performed a three-dimensional numerical simulation of snow drifting surrounding a 2m cubic obstacle. Zhou et al. (2014, 2016a) and Yu et al. (2019) employed the combined CFD and wind tunnel approach to simulate snowdrift patterns on flat and stepped roofs under various conditions. However, this CFD approach is computationally very intensive and even inappropriate for snow redistribution process modeling at watershed or basin scales for season-long simulations with significant uncertainty in land surface and weather conditions.

Larger scale snow distribution may be simulated by integrated microclimate, blowing snow, erosion and deposition of snow models (e.g., Lehning, et al (2008); Liston, et al (1998); Vionnet, et al (2014); Marsh, et al (2020)). However, watershed-scale snowdrift prediction can also be achieved by the wind modification parameter Sx that characterizes the degree of shelter or exposure of a point provided by the upwind terrain (Winstral and Marks, 2002; Winstral et al., 2002). This empirical parameterization was cost-effective when predicting snow distribution at the watershed scale (Erickson et al., 2005; Molotch et al., 2005; Schirmer et al., 2011; and Winstral et al., 2012). Schön et al. (2015, 2018) demonstrated that the estimates of the parameter Sx resulted in the successful delineation of the starting zones of small- and medium-sized avalanches in Col du Lac Blanc, France. It was still difficult to predict the starting point of extreme avalanches with very high return periods, especially with coarser than 10 m resolution (Veitinger et al., 2015). Parameterization of the wind-driven snow redistribution process based on topography and vegetation indices has been widely implemented in numerical models, such as Prairie Blowing Snow Model (PBSM) (Pomeroy et al., 1993; Essery et al., 1999), SnowTran3D/SnowModel (Liston and Sturm, 1998; Greene et al., 1999; Liston et al., 2007; Liston et al, 2018), SYTRON3 (Durand et al., 2005), Apine3D (Lehning et al., 2006; Lehning et

al., 2008; Mott et al., 2010), SnowDrift3D (Schneiderbauer and Prokop, 2011), and Meso-NH/Crocus (Vionnet et al., 2014). Fundamentally, these models are combinations of micro-meteorological wind modification and experimentally obtained snow transport formulations. However, the snow transport formulations available are not conclusive because of non-linearity in aerodynamic processes, variability in snow quality, and snow transport modes; therefore, considerable knowledge gap between wind field and snow particle motion still remains. As a result, the variation in snow transport estimates from wind speed can easily vary by multiple orders of magnitude depending on snow type and transport mode.

Macroscopic particle motion processes of snow particles can be described in terms of snow surface diffusion, advection, fetch, and eddies, which are functions of snow surface elevation. Some progress in this area was recently reported through the incorporation of classical process observations (e.g. Bagnold, 1941) through decoupling from the micro-meteorological wind field. For example, based on the snow transport formulas (e.g., Pomeroy and Gray, 1990), the snow particle dispersion coefficient was theoretically derived proportional to the autocorrelation length of wind friction speed (Ohara, 2014). The derived expression was incorporated in the FPE snow model to estimate the probability diffusion coefficient of snow depth (He and Ohara, 2019). Marsh et al., (2019) showed that the finite volume representation of the advection-diffusion blowing snow model with much simplified wind flow model can significantly reduce the computational requirement without sacrificing the snow distribution prediction ability. Ohara (2017) introduced a linear erosion term to the advection dispersion equation (the Linear Particle Distribution (LPD) equation), which can reproduce snow depth profiles affected by trees and perforated snow fences. He showed that the model based on the

LPD equation was effective for analyzing the snowdrift pattern around perforated snow fences and abrupt terrain features in wind-swept open terrains.

This study expands the use of the LPD equation for spatial snow distribution modeling with variously oriented snow fences over irregular terrain. In particular, it addresses two numerical issues: the artificial diffusion for advection instability, and the inner "boundary" condition of the snow fence in the middle of the modeling domain. To address the advection instability issue, the specialized numerical algorithm and the flux limiter method (e.g. Hirsch, 2007) have been implemented and tested using one-dimensional analytical exact solutions of the LPD equation, which are free from numerical artifacts. For the internal boundary condition issue, a combination of the "equivalent solid fence" and the "local erosion coefficient" modifications are introduced in this study. Finally, spatial model applications over representative real terrains are presented with corresponding snow depth measurements through manual probing, airborne LiDAR, ground penetrating radar (GPR), and UAV-based photogrammetry. We envision that this modeling approach will be particularly useful for diagnosing the snow particle motion processes from observable snowdrift patterns and for snowdrift prediction for watershed and regional scale applications at excellent computational efficiency.

## 2. Method

### 2.1 Linear Particle Distribution Equation

The mass conservation equation along the wind direction x on a one-dimensional horizontal surface can be written as:

$$\frac{\partial h}{\partial t} = -\frac{1}{\rho_p}\left[\frac{\partial Q}{\partial x} + f\right] \quad (1)$$

where $h$ is the relative snow surface height or simply snow depth in the case of flat terrain [L], $\rho_p$ is the density of particle deposit [M/L$^3$], $Q$ is the depth-integrated horizontal particle mass flux per unit width including snowfall and abrasion [M/T/L], $f$ is the vertical mass flux term describing snow precipitation, compaction, and abrasion [M/T/L$^2$], $x$ is the horizontal distance or length along the flow line [L] and $t$ is time [T]. Ohara (2017) parameterized the local snow particle flux difference ($\frac{\partial Q}{\partial x}$) using dispersion, advection, linear erosion, and snow mass exchange relating the snow surface elevation. The LPD equation for dynamic one-dimensional particle distribution as:

$$\frac{\partial h}{\partial t} = -\frac{1}{\rho_p}\left[a(x,t)\frac{\partial^2 h}{\partial x^2} + b(x,t)\frac{\partial h}{\partial x} + c(x,t)h + f(x,t)\right] \quad (2)$$

where $a$ is the mass dispersion coefficient [M/T/L], $b$ is the mass advection coefficient [M/T/L$^2$], and $c$ is the mass erosion coefficient [M/T/L$^3$]. When snow redistribution over an irregular terrain surface is discussed, the relative snow surface height $h$ is snow surface elevation from the datum such as the local average surface elevation. In practice, $h$ is snow surface elevation from a datum in the dispersion and advection terms while $h$ may be simply snow depth in the erosion term. The LPD equation is in the same form as the mathematical model of slope development proposed by Hirano (1968) and consists of dispersion, advection, erosion, and source terms. These particle motion parameters can be expressed as,

$$a = -\rho_p D \quad (3)$$

$$b = \rho_p \varphi \quad (4)$$

$$c = \rho_p \varepsilon \quad (5)$$

where $D$ is the surface diffusion coefficient or particle dispersion coefficient [L$^2$/T], $\varphi$ is wave migration velocity or celerity [L/T], and ε is the erosion coefficient [1/T]. Among these

parameters, the erosion coefficient was newly introduced by Ohara (2017) where linearity is assumed, which implies that the model parameters, diffusion, drift, and erosion coefficients, must be independent of the state variable $h$, the relative height of the surface. Also, snow density variation is not considered in Ohara (2017). Therefore, ignoring local snowfall and snowmelt during the drifting period ($f = 0$) to obtain an analytical solution, Equation (1) can be reduced to ,

$$\frac{\partial h}{\partial t} = D\frac{\partial^2 h}{\partial x^2} - \varphi\frac{\partial h}{\partial x} - \varepsilon h. \quad (6)$$

A useful analytical solution of this simplified LPD equation exists for one dimensional snowdrift profile.

## 2.2 Physical Significance of the LPD Equation

**2.2.1 Dispersion Coefficient:** the snow particle dispersion process is analogous to the well-established concept of the mass dispersion process known as Fick's 1st law. When the wind-driven redistribution of snow is discussed, snow surface diffusion or snow particle dispersion may be induced by the random fluctuation of snow particles. According to Ohara (2014), for a horizontal two-dimensional field, the diffusion coefficient of the blowing snow can be expressed as a time integration of the autocovariance function of the friction velocity of air. In practice, because the mean wind speed component is accounted for by snow particle advection, it is possible to reduce the correlation structure of the wind speed time series to the delta correlation. Thus, we have,

$$a = -\rho_p D = -\frac{\rho_{cv}}{h_{cv}}\int_0^T Cov[u_s(T)u_s(T-\tau)]d\tau$$

$$= -\frac{\rho_{cv}}{h_{cv}}k^{*2}\int_0^T Cov[u^*(T)u^*(T-\tau)]d\tau$$

$$= -\frac{\rho_{cv}}{h_{cv}}k^{*2}l_t \cdot Var(u^*)$$

where $u_s$ is snow particle speed; $u^*$ is the friction velocity of air or a representative wind speed; $T$ is the snow drifting time; $\tau$ is dummy variable for time for the integration; $k^*$ is the velocity-based snow drag coefficient; $\rho_{cv}$ is the density of blowing snow (mixture of snow and air) within a control volume with thickness of $h_{cv}$; and $l_t$ is the correlation length of snow particle speed. Despite the process-based formulation of the dispersion coefficient, there is considerable variation in control volume specifications depending on the mode of transport (e.g. suspension, saltation; see Table 1, Ohara, 2014; Aksamit et al., 2016). However, it is theoretically clear that the dispersion coefficient is proportional to the variance of wind speed during the period of time, T. Additionally, this snow surface diffusion is known as "curvature effect" because it depends on the snow surface curvature ($\frac{\partial^2 h}{\partial x^2}$) as showing in Equation (2). In other existing models (e.g. SNOWTRAN3D, Liston et al., 2007), the wind speed is empirically modified by the surface curvature to describe this effect.

**2.2.2 Advection Coefficient:** the advection coefficient $b(x,t)$ becomes equal to the mean snow particle travel speed when particles can travel freely within the air as suspended particles and saltation occurs over a relatively flat area. However, the advection coefficient typically corresponds to the celerity of the snow surface feature instead because the snow depth $h$ represents the spatial snow particle concentration. This downwind migration of snowdrift may be caused by erosion of windward slope erodes and deposits of leeward slope. On the other hand, snow dunes might possibly shift upward in the direction of the wind when saltating particles cannot easily climb over the hill. Therefore, the advection coefficient can be either positive or negative depending on the dominating mechanism of particle transportation; it is likely

proportional to the mean wind speed with positive coefficient ($\varphi \propto \bar{u}^*;\ \varphi > 0$). According to Ohara (2014), the advection coefficient can be written as

$$b = \frac{\rho_{cv}}{h_{cv}} \overline{u_s} = \frac{\rho_{cv}}{h_{cv}} k^* \cdot \bar{u}^* \tag{8}$$

where $\overline{u_s}$ is mean snow particle speed, and $\bar{u}^*$ is the mean friction velocity of air. Additionally, this effect is known as "slope effect" in the empirical snow redistribution modeling (Liston et al. 2007).

**2.2.3 Erosion Coefficient:** the linear erosion term, the third term in the right hand side of Equation (6), was introduced to describe the snow surface erosion as proportional to the snow depth relative surface elevation. The positive erosion coefficient $c(x,t)$ describes the initiation of blowing snow, called fetch process. As the erosion coefficient becomes smaller, the snow surface is hard to erode by wind. Hence, the erosion coefficient indicates how soft the snow is which is an important addition to the advection-dispersion model describing the snowdrift pattern around abrupt terrain features such as cliff and solid fence. Interestingly, although the erosion coefficient should intuitively remain positive, the negative erosion coefficient seems to be effective in describing the snowdrift observed around perforated objects such as trees and snow fences. Therefore, Ohara (2017) called it the fetch-eddy effect using the possible solution map of the LPD equations on the advection-erosion coefficient plane. Though the particle distribution (bedform) dynamics has often been considered a non-linear process (e.g. Andreotti et al., 2012; Csahók, et al., 2000), this liner erosion term is flexible enough to describe practically the snowdrift shape.

The linearity of the governing LPD equation provides a significant advantage in analyzing snow distributions using this framework. It is obvious that snowdrift shape $h(x,t)$ depends on the

relative magnitudes of three particle motion parameters ($D, \varphi, \varepsilon$ ) while the average magnitude determines the evolution speed (e.g. snow storm duration). In other words, the time-space scale invariant relationships are explicitly built-in. Moreover, even an analytical solution can be obtained with constant model parameters under the following initial and boundary conditions:

$$h(0,t) = h_o;\ t \geq 0 \tag{9}$$

$$h(x,t) \neq \infty\ ;\ x \to \infty, t \geq 0 \tag{10}$$

$$h(x,0) = 0\ ;\ x \geq 0 \tag{11}$$

where $h_o$ is a delta function which is the height of the snow fence at x = 0. Note that $h$ is the snow surface elevation that $h(x,t) = d(x,t) + z(x)$ where $d$(x,t) is snow depth and $z$(x) is surface elevation. The corresponding exact solution of the LPD equation (Equation 6) obtained by Ohara (2017) can be written as,

$$h(x,t) = \frac{h_o}{2}\exp\left(\frac{\varphi x}{2D}\right) \cdot \left[\exp\left(x\sqrt{\frac{\varphi^2}{4D^2}+\frac{\varepsilon}{D}}\right)\operatorname{erfc}\left(\sqrt{\frac{1}{4D}}\frac{x}{\sqrt{t}}+\sqrt{\frac{\varphi^2}{4D}+\varepsilon}\cdot\sqrt{t}\right)\right. + \left.\exp\left(-x\sqrt{\frac{\varphi^2}{4D^2}+\frac{\varepsilon}{D}}\right)\operatorname{erfc}\left(\sqrt{\frac{1}{4D}}\frac{x}{\sqrt{t}}-\sqrt{\frac{\varphi^2}{4D}+\varepsilon}\cdot\sqrt{t}\right)\right] \tag{12}$$

where

$$\operatorname{erfc}(x) = 1 - \operatorname{erf}(x)\ .$$

This analytical solution of the one-dimensional LPE is convenient for testing the numerical algorithm introduced as well as analyzing the snow surface diffusion, advection, and fetch/eddy effects in the downwind areas of various snow fences.

## 2.3 Numerical Algorithm

An appropriate two-dimensional numerical algorithm is required to simulate the spatial snowdrift patterns on highly irregular topography. A numerical algorithm of the advection-dispersion type equation unavoidably suffers from the convective instability for the high Péclet number cases. Numerical diffusivity (e.g., through up-winding) is typically introduced to overcome convective instability, but that is undesirable for snowdrift modeling because snowdrift was shown to be controlled by the relative magnitude of three effects: diffusion, advection, and fetch/eddy, as in the solution types mapped by Ohara (2017). To minimize numerical diffusivity, we adopted the flux limiter method (e.g., Hirsch, 2007) in this study.

The volume-based LPD equation for a two-dimensional spatial field can be written as,

$$\frac{\partial h}{\partial t} = D_x \frac{\partial^2 h}{\partial x^2} - \varphi_x \frac{\partial h}{\partial x} - \varepsilon_x h + D_y \frac{\partial^2 h}{\partial y^2} - \varphi_y \frac{\partial h}{\partial y} - \varepsilon_y h + \frac{f}{\rho_p} \tag{13}$$

where the subscripts denote spatial direction (x or y) and $f$ is the snow mass change due to snow precipitation and snow surface sublimation [M/L$^2$/T]. Note that the relative snow surface elevation can be decomposed as $h(x, y, t) = d(x, y, t) + z(x, y)$ where $d$ is snow depth and $z$ is ground surface elevation. Equation (11) can be discretized with a mixed finite difference-volume method as,

$$h_{i,j}^{n+1} = h_{i,j}^{n} + D_x \frac{\Delta t}{(\Delta x)^2}\left(h_{i+1,j}^{n} - 2h_{i,j}^{n} + h_{i-1,j}^{n}\right) - \frac{\Delta t}{\Delta x}\left(J_{i+\frac{1}{2},j}^{*} - J_{i-\frac{1}{2},j}^{*}\right) - \Delta t \varepsilon_x h_{i,j}^{n}$$
$$+ D_y \frac{\Delta t}{(\Delta y)^2}\left(h_{i,j+1}^{n} - 2h_{i,j}^{n} + h_{i,j-1}^{n}\right) - \frac{\Delta t}{\Delta y}\left(J_{i,j+\frac{1}{2}}^{*} - J_{i,j-\frac{1}{2}}^{*}\right) - \Delta t \varepsilon_y h_{i,j}^{n} + \Delta t \frac{\rho_w}{\rho_p} p \tag{14}$$

where superscript (n) denotes time step, subscript (i, j) denotes spatial grid number, $p$ is snow precipitation (m/s), $\rho_w$ is the density of water (1000 kg/m$^3$), $\Delta t$ is time increment, $\Delta x$ and $\Delta y$ are

spatial resolutions, and $J^*$ is snow particle flux due to advection. The snow particle flux of the advection terms in equation (11) between computational cells may be evaluated by,

$$J^*_{i+1/2,j} = \begin{cases} \varphi_x \, \tilde{h}^{\mathrm{W}}_{i+1/2,j} \; ; \varphi_x \geq 0 \\ \varphi_x \, \tilde{h}^{\mathrm{E}}_{i+1/2,j} \; ; \varphi_x < 0 \end{cases}$$
$$J^*_{i,j+1/2} = \begin{cases} \varphi_y \, \tilde{h}^{\mathrm{S}}_{i,j+1/2} \; ; \varphi_y \geq 0 \\ \varphi_y \, \tilde{h}^{\mathrm{N}}_{i,j+1/2} \; ; \varphi_y < 0 \end{cases} \tag{15}$$

where $\tilde{h}$ is the modified surface elevation with the flux limiter $\Phi$, and W, E, S, and N refer to the west, east, south, and north sides at the computational cell (*i, j*), respectively. The flux limiter can prevent spurious oscillations in the high order spatial discretization scheme due to sharp snow surface elevation discontinuities around a snow fence or a cliff. Based on the Monotonic Upstream-Centered Scheme for Conservation Laws (MUSCL) scheme (van Leer, 1979), the interface values between computational cells can be expressed as a linear extrapolation of the average values at the two upwind cells. They can be computed as

$$\tilde{h}^{\mathrm{W}}_{i+1/2,j} = h_{i,j} + \frac{1}{2}\Phi^{+}_{i-\frac{1}{2},j}\left(h_{i,j} - h_{i-1,j}\right), \qquad \tilde{h}^{\mathrm{E}}_{i+1/2,j} = h_{i+1,j} - \frac{1}{2}\Phi^{-}_{i+\frac{3}{2},j}\left(h_{i+2,j} - h_{i+1,j}\right),$$
$$\tilde{h}^{\mathrm{S}}_{i,j+1/2} = h_{i,j} + \frac{1}{2}\Phi^{+}_{i,j-\frac{1}{2}}\left(h_{i,j} - h_{i,j-1}\right), \qquad \tilde{h}^{\mathrm{N}}_{i,j+1/2} = h_{i,j+1} - \frac{1}{2}\Phi^{-}_{i,j+\frac{3}{2}}\left(h_{i,j+2} - h_{i,j+1}\right), \tag{16}$$

and

$$\Phi^{+}_{i-1/2} = \Phi(r^{+}_{i-1/2}), \qquad \Phi^{-}_{i+1/2} = \Phi(r^{-}_{i+1/2}). \tag{17}$$

The positive sign in the superscript means effective when the wave velocity $\varphi$ is positive while the negative superscript means effective when the wave velocity $\varphi$ is negative. The limiters are required to eliminate numerical oscillations. The ratio between successive gradients, *r*, can be estimated by

$$r^{+}_{i-\frac{1}{2},j} = \frac{h_{i+1,j}-h_{i,j}}{h_{i,j}-h_{i-1,j}}, \qquad r^{-}_{i+\frac{3}{2},j} = \frac{h_{i,j}-h_{i+1,j}}{h_{i+1,j}-h_{i+2,j}},$$
$$r^{+}_{i,j-\frac{1}{2}} = \frac{h_{i,j+1}-h_{i,j}}{h_{i,j}-h_{i,j-1}}, \qquad r^{-}_{i,j+\frac{3}{2}} = \frac{h_{i,j}-h_{i,j+1}}{h_{i,j+1}-h_{i,j+2}}. \tag{18}$$

Through comparisons among the flux limiters, Van Leer's (Van Leer, 1974), min-mod (Roe, 1986), superbee (Roe and Baines, 1982), and MUSCL limiter (Van Leer, 1979), the MUSCL limiter provided the best performance for bell-shaped solutions. The MUSCL limiter (Van Leer, 1979), which can be expressed as,

$$\Phi(r) = \max[0, \min(2r, (r+1)/2, 2)], \tag{19}$$

was selected for use in this study. This numerical algorithm was implemented in the SMOOTH model platform (Ohara, 2014).

## 2.4 Validation of the Numerical Algorithm in 1D Snow Profiles

The numerical solutions were verified by the one-dimensional analytical (exact) solution, presented in Equation (11), around a snow fence, to check how well anticipated numerical diffusion is suppressed. Figure 1 shows the two demonstrative numerical simulation results and the corresponding analytical (exact) solutions (Equation 11) for both positive (upper panel) and negative (lower panel) erosion coefficient cases. The Dirichlet boundary condition (DBC) (at the upstream end with the snow fence unit height $h(0)$ = 1.0m) was used for both model verification cases. Note that the positive erosion coefficient represents the snowdrift around a solid fence while the negative one corresponds to the perforated snow fence case (Ohara, 2017). The effect of perforated fence must be eliminated when snow surface reaches the physical fence top.

The accuracy of the numerical algorithm was measured by the root-mean-square deviation (RMSD) and the Nash–Sutcliffe model efficiency (NSE), displayed in Figure 1. The differences were very small for both cases, although a slightly larger error was found in the negative erosion coefficient case (lower). It can be concluded that the numerical algorithm

presented above effectively limits the anticipated convective instability without introducing numerical diffusivity.

[Insert Figure 1 ]

## 3. Applications

Realistic snow particle motion parameters for the SMOOTH model are discussed in this section using the state-of-art observed snow distributions in several representative terrains in Southeast Wyoming and Northern Alaska, where wind dominates snow distribution. Ideally, these physical model parameters should be estimated from wind and snow drag characteristics. However, since the dynamic snow motion information is hardly accessible in reality, the model is used as a tool in this study to gain insight into the physical processes through the extensive calibration to the observed snow distribution data assuming uniform and stationary model parameters for each application.

### 3.1 One-dimensional simulation for snow fences

Since snow fences are an effective tool to alter snowdrift patterns for easier road maintenance and local water resource enhancement, snowdrift distributions have been studied in the literature (e.g. Tabler, 1986; Wangstorm, 1989; Hinkel et al. 2006; Sturm and Stuefer, 2013; Stuefer and Kane, 2016). For example, Tabler (e.g., 2003), over decades, documented numerous snowdrift patterns around various snow fence types mainly in Wyoming and synthesized all available snowdrift profiles along the prevailing wind stream line. The snowdrift pattern around perforated snow fences is an excellent first step toward understanding the effects of irregular topography and vegetation on snow distribution. The LPD equation successfully described the

snowdrift patterns downstream from various snow fences with the DBC at the upstream end (Ohara, 2017). However, the DBC is inappropriate for snowdrift simulation with a snow fence in the middle of the computational domain. The snowdrift can be described by an equivalent elevation lift of the terrain, called "equivalent solid fence" in this study. Snowdrift distribution associated with this equivalent solid fence may be modified by an eddy effect brought about by the negative erosion coefficient for the perforated fence in the middle of the domain. This treatment of the inner "boundary" condition is required for variously oriented snow fences on irregular two-dimensional terrain. The equivalent height of the perforated snow fence may not be determined by physical properties but by model calibration in this study. In this section, the new equivalent solid snow fence, which results in the same snowdrift pattern as the perforated snow fence, is discussed.

In addition to the three particle motion parameters, the snowdrift around a snow fence can be described by two additional parameters: the height of the equivalent solid fence and the length of the influenced area. Figure 2 illustrates the proposed equivalent snow fence configuration with modification in the fetch-eddy effect (erosion coefficient). The dispersion and the advection coefficients may be assumed to be less sensitive to the snow fence influence while the erosion coefficient may be considerably modified by the snow fence. In fact, Ohara (2017) showed that the negative linear erosion coefficient can result in the single peaked snowdrift around a perforated snow fence due to turbulence created by the fence. In this study, therefore, the negative erosion coefficient was applied only downstream of the fence while it was set at zero for the rest of the area to limit unnecessary snowdrift elsewhere. To determine the area influenced by the fence, the advection coefficient $b$, which represents the wind direction, was used in the numerical model. Thus, the snowdrift around the snow fence in the middle of the

computational domain was described by three parameters: the height of the equivalent solid fence, the length of the influenced area, and the erosion coefficient c in the influenced area.

[Insert Figure 2]

.

Figure 3 illustrates the comparison between the SMOOTH model output and the synthesized, field-observed snowdrift profiles (Tabler, 2003) both upstream and downstream of solid and perforated snow fences. Note that porosity (open area between fence slats), which is expressed as a proportion of the total fence area, is a design parameter of a snow fence. The snow-free initial condition ($h = 0$) is adopted while the flat Neumann Boundary Condition (NBC) ($dh/dx = 0$) are given for both ends of the computational domain. Since the spatial and vertical scale was normalized for the snow fence height, snow fence height was set to 1 in this figure. The corresponding equivalent snow fence heights for the perforated snow fences as well as the other parameters $a$, $b$, and $c$ were determined by automated trial-and-error iterations (grid search). The model parameters are shown on the corresponding panels of Figure 3, and the length of the area influenced by the fence is 50 m. The snowdrift areas in the upstream as well as the downstream sections show very good agreement. Therefore, model configuration with a snow fence in the middle domain was found to be effective in one-dimensional cases.

[Insert Figure 3]

### 3.2 Two-dimensional simulations with and without snow fences

Here we applied the SMOOTH model to snow distributions on actual irregular terrain in the Laramie Range (Figure 4) using LiDAR-observed snow depth data from April 2016 available through previous work (e.g., He et al., 2019). Further, the airborne LiDAR system produced scans with and without snow cover during 2014 and 2016, respectively, and differentiating them yielded the snow depth map at 0.5 m spatial resolution with +/- 1 cm accuracy. Four rectangular model domains within the region were selected for the model demonstration.

[Insert Figure **4**]

Figure 5 illustrates the model calibration and validation results for snow fenced areas along Interstate 80 (I-80). The model parameters are on the upper right corner and the error measure (RMSD) are on the left panels [(a) and (e)] of Figure 5. NSE was omitted for the natural terrain applications because the no-snow areas often mislead the NSE model performance evaluation. The snow-free initial condition ($h = z$) and the flat NBC ($dh/dx = 0$) for all ends of the computational domain are used. The standard Wyoming-type perforated fences in the Malody and Honey Tree areas are approximately 3-4 m tall and to the west of I-80. The equivalent snow fence height of 1.3 m which is slightly higher value than the 1D runs was adopted because of irregularity and roughness effect of the terrain. Although westerly wind is expected in this area, the model was calibrated by the grid-search method without using wind information. Nonetheless, the advection in the southerly direction ($b_y$) was determined to be zero while the observed prevailing wind direction (wind rose in Figure 5) was westerly during the snow accumulation period of the 2016 season (December 2015 – April 2016). Hence, it is

reasonable to estimate the advection coefficient from the wind direction record. Panel (d) shows the 50 m-long area of influence downstream from the fence. Even though accuracy in the validation run in the Honey Tree site (RMSD=0.76 m) dropped compared to the calibration run in the Malody site (RMSD=0.41 m), the SMOOTH model reproduced the snowdrift patterns around the snow fences. Differences were found mainly around I-80 where snow plowing and snowmelt enhancement by deicing measures (salt and sand) may have had an effect.

[Insert Figure 5]

Figure 6 compares the SMOOTH model outputs to the LiDAR-observed snow depth map at the other two sites; Dale Creek for the open riparian zone, and Blair Wallis for the partial forest cover. The Dale Creek model was calibrated independently for all seven parameters ($a_x$, $b_x$, $c_x$, $f$, $a_y$, $b_y$, $c_y$) by the grid-search method to verify SMOOTH model description accuracy of snowdrift patterns in a hydrologically important riparian zone (Figure 6). The parameters for the Dale Creek and Blair Wallis sites were slightly different from the snow fence sites; snow patterns in the open areas can be reproduced well without the eddy effect (zero erosion coefficients $c_x$ and $c_y$). Considering that running SMOOTH requires very-little computational power (only a few minutes with a standard desktop PC for each run), this model is a robust cost-effective tool to quantify the highly heterogeneous snowmelt water input to the riparian hydrological system. This may be particularly significant because LiDAR data is available for only a few selected areas during calm periods.

The same model configuration was applied to the Blair Wallis site as shown in panels (d) through (f) of Figure 6. Despite the validation run, the RMSD value for the Blair Wallis site

(RMSD=0.19) was smaller than the calibration run for the Dale Creek site (RMSD=0.46) because the Dale Creek area had shallower average snow cover due to smoother terrain despite the presence of sparse forest cover. However, the snowdrift associated with the patchy forested area at Blair Wallis may not be reproduced very well, although the snow patterns due to the topography were well expressed by the model. Because vegetation growth is mainly limited by water supply from snowmelt in this region, quantification of turbulence generated by the vegetation will be important to assess synergy between vegetation and snowdrift. Clearly, snow redistribution is not insignificant in windy regions like Wyoming.

[Insert Figure 6]

### 3.3 Snowdrift Profile Around the Lakeshore Cliff of a Frozen Thermokarst Lake in Alaska

The SMOOTH model was applied to the snowdrift profile imaged with GPR (Malå ProEx, 250Mhz, GuidelineGeo, Sundbyberg, Sweden) around a natural lakeshore cliff of a thermokarst lake at Inigok, North Slope, Alaska (70.00134° N, 153.06758° W). The snowdrifts that develop on steep slopes surrounding thermokarst lakes in these regions are a critically important component of the water budget, and provide water storage on the land surface late into the melt season, yet they are poorly quantified (Sturm and Liston, 2003). Figure 7 shows this model application for a snowdrift induced by steep terrain in the absence of surface vegetation with the NBC. The GPR data were collected on 22 April 2016 near maximum snowpack conditions and the data were processed in ReflexW (Sandmeier Software, Karlsruhe, Germany) using dewow and a linear gain with topographic correction adapted from the ArcticDEM. The

GPR can image the stratigraphy in the snowpack due to the different relative dielectric permittivity of the layers (Davis and Annan, 1989; Neal, 2004). The reflections that occur due to density differences caused by snow metamorphism and freeze-thaw cycles may be regarded as a historical snow surface (e.g., Annan et al., 1994). Therefore, the snowdrift model was sequentially calibrated from the bottom reflection line (rflex4) to the shallower reflection line (rflex1) toward the snow surface by the grid-search method. The flat NBC and the snow-free initial condition were applied. Referring to the model parameters determined in Table 1, the parameters are different between snow accumulation periods. This implies the snow particle motion parameters varied during this single snow drifting season. Especially, the erosion coefficient c started with negative during early season while it approached to zero as the surface was smoothened by the snowpack development. Given the approximate resolution of this GPR instrument is ~0.2 m, the model was able to reproduce all reflections within measurement uncertainty (Table 1). However, the model for lower layers (rflex1 ~ 4) required a negative source parameter ($f < 0$) that indicates uniform snow depth reduction during the period to fit the model simulations to the observations. This source term was originally introduced for snow depth thickening due to new incoming snowfall during the simulation period. The model application indicates that uniform snow compaction and abrasion prevailed over snow accumulation in this cliff section, and most of the snow was likely formed by drifted snow from upwind. Additionally, snow surface hardening effect between the sequential runs was described by erosion limitation of the previous snow surface. This application suggests that some missing model components such as snow densification might improve the predictability of snowdrift thickness; snow metamorphism and snowdrift event history clearly influence model performance.

[Insert Figure 7]

[Insert Table 1]



## 3.4 Spatial snow distribution in the Arctic

Snowdrifts affect the thermal regime of permafrost because a relatively thick snowpack can effectively insulate the permafrost from cold winter air temperatures of the Arctic (Stieglitz et al. 2003) and result in warmer subsurface temperatures. Conversely, snow that persists well into the summer reduces the period of soil warming and diminishes heat flow to depth. This efficient numerical algorithm for the LPD equation could be an ideal tool for two-dimensional snowdrift modeling over complex terrains with sparse or negligible vegetation such as the Arctic Coastal Plain in northern Alaska. A demonstrative preliminary model output around a drained thermokarst lake basin referred to as Central Marsh, part of the Circumpolar Active Layer Monitoring (CALM) Network (N71.30259° N, 156.60075° W, 2.93 $km^2$) east of Utqiaġvik, Alaska, is shown in Figure 8. The snow-free terrain model was prepared using UAV photogrammetry techniques on 04 August 2019 at 0.25 m spatial resolution. The snow depth distribution was measured on 15 April 2019 using the same UAV photogrammetry technique, as shown in Figure 8 (left panel marked as "Obs.") (Nichols, 2020). All images were collected with a Phantom 4 UAV (P4RTK) and post-processed/georeferenced to NAD83 Zone 4 North in Ellipsoid heights using a propeller aeropoint and Pix4D (version 4.3.33 for April survey, 4.4.12 for August). A spatial resolution of 25 cm was selected during post-processing, as this achieved a good balance of resolution and file size. DEM creation was done in Quick Terrain Modeler (QTM) with the densified point cloud from Pix4D. The vertical accuracy of the dataset is a

product of the structure-for-motion (SfM) software. Vertical accuracy for the April survey was 18 cm and 10 cm for the August survey.

The simulated and UAV-observed snow accumulation pattern is consistent with the development of seasonal snow along drained lake basin, lake, river and coastal shorelines in this region (Konig and Sturm, 1998; Benson and Sturm, 1993; Sturm and Liston, 2003) as well as ice wedge troughs and pits (Liljedahl et al. 2016). The optimum model parameter combination was determined by more than 13,000 iterative simulations through a grid search using a desktop computer (Intel Core i7-4790K, Quad-Core 4.0GHz); each season-long computation takes only a few minutes. After the calibration exercise, the model reproduced the snowdrift pattern at RMSD of 0.115 m. The advection coefficients ($b_x$ = -0.001 and $b_y$ = 0.000) indicate an easterly wind, which is the prevailing winter wind direction. The erosion coefficients in both directions were calibrated as zero, which implies that the advection-dispersion model is sufficient to model the snowdrift in snow-fence or vegetation-free environments. This SMOOTH model can interpolate and possibly extrapolate the observed seasonal snow distributions over any windy open areas including the Arctic, where it is difficult to operate the UAV or even ground-based systems during most of the winter season. Additionally, the modeled snow depth (right panel in Figure 8) can resolve the detailed snowdrift structure affected by polygonal patterned ground, widespread ice-wedge polygons in the Arctic tundra.

[Insert Figure 8]

## 4. Discussion

The field-observed snow distribution patterns were analyzed by the improved SMOOTH model, a model that can partition the various effects such as: diffusion, advection, and fetch/eddy

effects, over the winter season. For this purpose, the numerical scheme in the SMOOTH model must be free from numerical viscosity (artificial diffusion). The analytical (exact) solutions for the downstream sections of snow fences with the DBCs were very useful for testing the numerical code. It is well known that the over-diffused numerical scheme (e.g. upwind finite difference (FD) scheme) is an effective aid against convective instability. As such, it demonstrated the utility of the MUSCL numerical scheme as a flux limiter method, which hybridizes the upwind FD and the higher order discretization. The MUSCL scheme was successfully implemented in the SMOOTH model because it was able to reproduce the exact solutions of the LPD equation under any realistic parameter combinations as demonstrated in Figure 1. Hence, the calibrated 2D models for the observed high-quality snow distribution data in Wyoming and Alaska can explain the physical processes acted during the accumulation period.

Linearity of the governing LPD equation provides a substantial advantage in interpretation of the simulation results and the determined particle motion parameters (diffusion, advection, and erosion coefficients). According to Ohara (2017), the snowdrift profile shape is mainly determined by the relative magnitude of the particle motion parameters while the average magnitude controls the evolution speed, assuming that most snowdrifts in natural terrain are considered in a transient state. For example, doubling all particle motion parameters results in a two-times faster snowdrift development without changing its overall shape. The demonstrative model applications presented here used a typical, estimated season total snowstorm duration in the regions for the model calibrations. Therefore, if the winter period weather condition is available, it is possible to adjust the snowdrifting period or snowstorm duration by scaling the parameters while the relative magnitude of the parameters remain valid. Figure 9 shows the

fractional magnitudes of the particle motion parameters for various applications presented in this study. The magnitudes were evaluated using the Pythagorean theorem for two-dimensional cases. This analysis illustrates similarity among snowdrift patterns around the solid fence (d), Dale Cr. (f), and Inigok (g) with significant contribution of advection effect due to the abrupt change in surface elevation. On the other hand, the perforated snow fences (a), (b), and (c) clearly require the fetch/eddy effect with minimum advection effect. The two-dimensional snow fence case (e) is somewhere between the abrupt elevation change and the perforated snow fence cases, suggesting that both effects of the natural terrain and the snow fence affect the snow distribution even with the fence influence area consideration. Overall, the diffusion effect dominates the snow redistribution in the open terrains over the other two effects. Especially, the snow distribution in the relatively mild terrain of the CALM grid was almost entirely driven by the diffusion effect. This result suggests that incorporation of diffusion effect may suffice in watershed or regional scale snow modeling for snow redistribution unless snowdrift patterns around perforated objects or sharp terrain transition are of interest. At least, the advection dispersion model should be adequate for most natural, relatively smooth terrains without significant surface roughness, forest, or perforated snow fences. Consequently, the erosion coefficient is an optional freedom to the model configuration unless surface roughness or steep terrain affects snowdrift patterns.

Despite the highly dynamic atmospheric system affecting the snow redistribution (Aksamit and Pomeroy, 2016), the case studies presented here showed solid performance of the model with the spatially uniform time-averaged model parameters after the calibration to the ground truth snow distributions. This indicates that three macroscopic snow particle motion effects in two directions (total 6 parameters) were capable to describe the time-integrated wind

driven snow redistribution processes represented by the observable snow distribution in these areas. The two main parameters, snow surface diffusion and advection coefficient, could be estimated from wind data as they were values consistent with the prevailing wind data. Generally, the advection coefficient agreed well with the prevailing mean wind direction, while the diffusion coefficient along the prevailing wind direction was larger than the lateral direction. Although the snow particle motion parameters clearly depend on the prevailing wind field, spatially uniform time-averaged values can successfully reproduce snow distribution patterns affected by topography.

The SMOOTH model is a decoupled or stand-alone snow redistribution model from the wind or blowing snow modeling unlike other integrated physically-based models (Lehning, et al., 2008; Liston, et al., 1998; Vionnet, et al., 2014; Marsh, et al., 2020). Therefore, the required input data is simply a digital elevation model, which may include abrupt terrain and snow fences. This simple decoupled model offers quick solutions within a few seconds to minutes by a standard PC even for the CALM case (1680 x 1743, 1 meter resolution). Therefore, many iterative simulations for searching the best parameter combination are possible if snow depth data are available; this data can be easily integrated in the distributed snowmelt model. Additionally, the time-averaged particle motion parameters determined by model calibration are a useful checkpoint at the interface of the microclimate and snow dynamics because there is considerable uncertainty in wind and blowing snow modeling. Finally, since the original form of the model formulation is very general (e.g. time-space dependent model parameters), the SMOOTH model can be easily expanded for a fully dynamic simulation of snowdrift when a better model parameter estimation method associated with dynamic wind field becomes available.

Snow trapping by vegetation likely enhances spring season water input which is essential for plant growth (Sturm et al 2001). Therefore, an understanding of this process is crucial for synergistic feedback between snowpack and ecosystems. However, to effectively model snowdrifts around vegetation or any irregular surface roughness, additional study is needed to determine the snow particle motion parameters (dispersion, advection, and erosion coefficients) and is beyond this proposed modeling framework. Also, through the snowdrift simulation for the steep cliff in Inigok, AK (Figure 7 and Table 1), uniform snow depth decrease ($f < 0$) was unavoidable to match the model to the measured internal reflection lines of the snowpack. This suggested a missing model component, such as snow densification, in the current version. Nevertheless, the model applications suggest the possibility of snowdrift simulation around more complex and irregular perforated objects, such as vegetation and patchy forest on the irregular terrain by the Eulerian approach.

## 5. Conclusions

The two-dimensional numerical SMOOTH model, based on the LPD equation, was shown to be applicable and practical for snowdrift prediction in windy open terrains. Model calibration and validation exercises demonstrated steadiness in snowdrift simulations with and without the perforated snow fences in the Laramie Range, Wyoming. It can therefore be concluded that this model is a valid, cost-effective tool for snowdrift prediction associated with the forecasted-wind fields based on the physically-based predictive equation. Moreover, these model implementations indicate the possibility of estimating snow particle motion parameters

from resultant snow distribution. The calibrated snow particle motion parameters and the computational conditions provide insights for understanding the snow redistribution process.

Overall, the remaining known challenges to the physically-based Eulerian snowdrift prediction may be summarized as follows: 1) the particle motion parameters may be dynamic (time dependent) and heterogeneous (spatially distributed) in nature; 2) better snowpack dynamics modeling, such as snow densification and abrasion, affecting the model predictions should be incorporated; 3) appropriateness of the fetch/eddy effect parameterization is still largely unknown despite the successful demonstrations presented here.

Efforts applied to understand physically-based modeling is of fundamental importance in elucidating snowpack dynamics. For example, such a model could estimate associated parameters from field-observed particle distributions, which would have physical implications. This developed model can incorporate any new knowledge explicitly or be incorporated into the greater modeling framework directly. The applicability of the SMOOTH model demonstrated here is encouraging and useful for understanding the hydrological cycles in wind swept open areas such as the high plains of the Rocky Mountains and the tundra in Arctic regions.

## ACKNOWLEDGEMENTS

This study was supported by the National Science Foundation (NSF) under awards EPS-1208909 and OPP- 1806287, 1806213, and 1806202. The authors thank UIC Science and CH2MHill Polar Field Services (now Battelle Arctic Research Operations) for field logistical support.

## Data Availability Statement

Source code of SMOOTH model and input datasets that support the findings of this study are available in the Mountains Scholar at https://mountainscholar.org/handle/20.500.11919/7146 [http://dx.doi.org/10.15786/20.500.11919/7146]. The Lidar snow depth data are available in the Mountains Scholar at https://mountainscholar.org/handle/20.500.11919/3575 [https://dx.doi.org/10.15786/M2PD5Q].

## REFERENCES

Aksamit, N. O., & Pomeroy, J. W. (2016). Near-surface snow particle dynamics from particle tracking velocimetry and turbulence measurements during alpine blowing snow storms. The Cryosphere, 10(6), 3043-3062.

Andreotti, B., Claudin, P., Devauchelle, O., Durán, O., & Fourrière, A. (2012). Bedforms in a turbulent stream: ripples, chevrons and antidunes. Journal of Fluid Mechanics, 690, 94-128.

Annan, A. P., Cosway, S. W., & Sigurdsson, T. (1994). GPR for snow pack water content. In *Fifth International Conference on Ground Penetrating Radar* (pp. cp-300). European Association of Geoscientists & Engineers.

Anno, Y. (1984). Requirements for modeling of a snowdrift. *Cold regions science and technology*, *8*(3), 241-252.

Bagnold, R. A. (1941). The physics of blown sand and desert dunes: New York. William Morrow & Company.

Benson, Carl S., and Matthew Sturm. "Structure and wind transport of seasonal snow on the Arctic slope of Alaska." Annals of Glaciology 18 (1993): 261-267.

Beyers, J. H. M., Sundsbø, P. A., & Harms, T. M. (2004). Numerical simulation of three-dimensional, transient snow drifting around a cube. Journal of Wind Engineering and Industrial Aerodynamics, 92(9), 725-747.

Bisht, G., Riley, W. J., Wainwright, H. M., Dafflon, B., Yuan, F., & Romanovsky, V. E. (2018). Impacts of microtopographic snow redistribution and lateral subsurface processes on hydrologic and thermal states in an Arctic polygonal ground ecosystem: a case study using ELM-3D v1. 0. Geoscientific Model Development (Online), 11(1).

Blöschl, G. (1999). Scaling issues in snow hydrology. Hydrological processes, 13(14‐15), 2149-2175.

Csahók, Z., Misbah, C., Rioual, F., & Valance, A. (2000). Dynamics of aeolian sand ripples. The European Physical Journal E, 3(1), 71-86.

Cline, D., Elder, K., & Bales, R. (1998). Scale effects in a distributed snow water equivalence and snowmelt model for mountain basins. Hydrological Processes, 12(10‐11), 1527-1536.

Dadic, R., Mott, R., Lehning, M., & Burlando, P. (2010). Wind influence on snow depth distribution and accumulation over glaciers. *Journal of Geophysical Research: Earth Surface*, *115*(F1).

Davis, J. L., and Annan, A. P. (1989). Ground-penetrating radar for high-resolution mapping of soil and rock stratigraphy. *Geophysical prospecting*, 37, 531–551.

Deems, J. S., Fassnacht, S. R., & Elder, K. J. (2006). Fractal distribution of snow depth from LiDAR data. *Journal of Hydrometeorology*, *7*(2), 285-297.

Durand, Y., Guyomarc'h, G., Mérindol, L., & Corripio, J. G. (2005). Improvement of a numerical snow drift model and field validation. *Cold regions science and technology*, *43*(1-2), 93-103.

Erickson, T. A., Williams, M. W., & Winstral, A. (2005). Persistence of topographic controls on the spatial distribution of snow in rugged mountain terrain, Colorado, United States. *Water Resources Research*, *41*(4).

Essery, R. L. H., L. Li, and J.W. Pomeroy (1999), A Distributed Model of Blowing Snow over Complex Terrain. *Hydrol. Process*., 13, 2423–2438.

Greene, E.M., G.L. Liston and R.A. Pielke (1999), Simulation of above treeline snowdrift formation using a numerical snow-transport model. *Cold Reg. Sci. Technol.*, 30(1–3), 135–144.

Grünewald, T., Schirmer, M., Mott, R., & Lehning, M. (2010). Spatial and temporal variability of snow depth and SWE in a small mountain catchment. *The Cryosphere*, *4*(ARTICLE), 215-225.

He, S., & Ohara, N. (2019). Modeling Subgrid Variability of Snow Depth Using the Fokker-Planck Equation Approach. *Water Resources Research*, *55*(4), 3137-3155.

He, S., Ohara, N., & Miller, S. N. (2019). Understanding subgrid variability of snow depth at 1‐km scale using Lidar measurements. Hydrological Processes, 33(11), 1525-1537.

Hinkel, K. M., & Hurd Jr, J. K. (2006). Permafrost destabilization and thermokarst following snow fence installation, Barrow, Alaska, USA. Arctic, Antarctic, and Alpine Research, 38(4), 530-539.

Hirano, M. (1968). A mathematical model of slope development: an approach to the analytical theory of erosional topography. Journal of Geosciences Osaka City University, (11), 13-52.

Hirsch, C. (2007). *Numerical computation of internal and external flows: The fundamentals of computational fluid dynamics*. Elsevier.

Iversen, J. D. (1980). Drifting-snow similitude—transport-rate and roughness modeling. Journal of glaciology, 26(94), 393-403.

Kind, R. J. (1976). A critical examination of the requirements for model simulation of wind-induced erosion/deposition phenomena such as snow drifting. *Atmospheric Environment (1967)*, *10*(3), 219-227.

Kind, R. J. (1986). Snowdrifting: a review of modelling methods. *Cold Regions Science and Technology*, *12*(3), 217-228.

Kind, R. J., & Murray, S. B. (1982). Saltation flow measurements relating to modeling of snowdrifting. *Journal of Wind Engineering and Industrial Aerodynamics*, *10*(1), 89-102.

Kuchment, L. S., & Gelfan, A. N. (2001). Statistical self-similarity of spatial variations of snow cover: verification of the hypothesis and application in the snowmelt runoff generation models. *Hydrological Processes*, *15*(18), 3343-3355.

König, M., & Sturm, M. (1998). Mapping snow distribution in the Alaskan Arctic using aerial photography and topographic relationships. Water Resources Research, 34(12), 3471-3483.

Lehning, M., I. Völksch, D. Gustafsson, T.A. Nguyen, M. Stähli, and M. Zappa (2006), ALPINE3D: a detailed model of mountain surface processes and its application to snow hydrology. *Hydrological Processes*, 20(10), 2111-2128.

Lehning, M., Löwe, H., Ryser, M., & Raderschall, N. (2008). Inhomogeneous precipitation distribution and snow transport in steep terrain. *Water Resources Research*, *44*(7).

Liston. G.E., R.B. Haehnel, M. Sturn, C.A. Hiemstra, S. Berezovskaya, and R.D. Tabler, (2007), Instruments and Methods Simulating complex snow distributions in windy environments using SnowTran-3D. Journal of Glaciology, vol. 53, Issue 181, 241-256.

Liston, G. E., Polashenski, C., Rösel, A., Itkin, P., King, J., Merkouriadi, I., & Haapala, J. (2018). A Distributed Snow-Evolution Model for Sea- Ice Applications (SnowModel). *Journal of Geophysical Research: Oceans*, *123*(5), 3786-3810.

Liston, G. E., & Sturm, M. (1998). A snow-transport model for complex terrain. Journal of Glaciology, 44(148), 498-516.

Marsh, C. B., Pomeroy, J. W., Spiteri, R. J., & Wheater, H. S. (2020). A finite volume blowing snow model for use with variable resolution meshes. Water Resources Research, 56(2), e2019WR025307.

Molotch, N. P., Colee, M. T., Bales, R. C., & Dozier, J. (2005). Estimating the spatial distribution of snow water equivalent in an alpine basin using binary regression tree models: the impact of digital elevation data and independent variable selection. *Hydrological Processes: An International Journal*, *19*(7), 1459-1479.

Moon, W., Nandan, V., Scharien, R. K., Wilkinson, J., Yackel, J. J., Barrett, A., ... & Duke, P. J. (2019). Physical length scales of wind-blown snow redistribution and accumulation on relatively smooth Arctic first-year sea ice. *Environmental Research Letters*, *14*(10), 104003.

Mott, R., and M. Lehning (2010), Meteorological modeling of very high-resolution wind fields and snow deposition for mountains. *J. Hydrometeorol*. 11 (4), 934–949.

Mott, R., Schirmer, M., & Lehning, M. (2011). Scaling properties of wind and snow depth distribution in an Alpine catchment. *Journal of Geophysical Research: Atmospheres*, *116*(D6).

Mott, R., Vionnet, V., & Grünewald, T. (2018). The seasonal snow cover dynamics: review on wind-driven coupling processes. Frontiers in Earth Science, 6, 197.

Neal A. (2004). Ground-penetrating radar and its use in sedimentology: principles, problems and progress. *Earth-Science Reviews*, 66, 261–330.

Nichols, I.O. (2020). *Assessing the Accuracy of a UAV Snow Depth Survey Utqiagvik (Barrow), Alaska Calm Grid*, M. S. Thesis, Geological Engineering, Michigan Technological University.

O'Rourke, M., DeGaetano, A., & Tokarczyk, J. D. (2004). Snow drifting transport rates from water flume simulation. *Journal of wind engineering and industrial aerodynamics*, *92*(14-15), 1245-1264.

O'Rourke, M. (2010). Snow Loads: Guide to the Snow Load Provisions of ASCE 7-10. American Society of Civil Engineers.

Ohara, N. (2014). A practical formulation of snow surface diffusion by wind for watershed scale applications. Water Resources Research, 50(6):5074-5089.

Ohara, N. (2017). An Eulerian equation for snow accumulation downstream of an object. Water Resources Research, 53(2):1525-1538.

Oikawa, S., Tomabechi, T., & Ishihara, T. (2007). Study of wind tunnel similarity on snowdrift around buildings. *J Snow Eng Jpn*, *23*(2), 13-32

Pomeroy, J. W., & Gray, D. M. (1990). Saltation of snow. Water resources research, 26(7), 1583-1594.

Pomeroy, J.W., D.M. Gray, and P.G. Landine (1993), The Prairie Blowing Snow Model - characteristics, validation, operation. *J. Hydrol*., 144, 165–192.

Roe, P. (1986). Characteristic-based schemes for the euler equations. Annual review of fluid mechanics, 18(1):337-365.

Roe, P. and Baines, M. (1982). Algorithms for advection and shock problems. In Numerical Methods in Fluid Mechanics, pages 281-290.

Schirmer, M., Wirz, V., Clifton, A., & Lehning, M. (2011). Persistence in intra-annual snow depth distribution: 1. Measurements and topographic control. *Water Resources Research*, *47*(9).

Schneiderbauer, S., & Prokop, A. (2011). The atmospheric snow-transport model: SnowDrift3D. *Journal of Glaciology*, *57*(203), 526-542.

Schön, P., Naaim-Bouvet, F., Vionnet, V., & Prokop, A. (2018). Merging a terrain-based parameter with blowing snow fluxes for assessing snow redistribution in alpine terrain. *Cold Regions Science and Technology*, *155*, 161-173.

Schön, P., Prokop, A., Vionnet, V., Guyomarc'h, G., Naaim-Bouvet, F., & Heiser, M. (2015). Improving a terrain-based parameter for the assessment of snow depths with TLS data in the Col du Lac Blanc area. *Cold Regions Science and Technology*, *114*, 15-26.

Stieglitz, M., Déry, S. J., Romanovsky, V. E., & Osterkamp, T. E. (2003). The role of snow cover in the warming of arctic permafrost. Geophysical Research Letters, 30(13).

Stuefer, S. L., & Kane, D. L. (2016). Snow retention for increased water supply of shallow Arctic lakes. Cold Regions Science and Technology, 123, 32-43.

Sturm, M., Holmgren, J., McFadden, J. P., Liston, G. E., Chapin III, F. S., & Racine, C. H. (2001). Snow–shrub interactions in Arctic tundra: a hypothesis with climatic implications. Journal of Climate, 14(3), 336-344.

Sturm, M., & Liston, G. E. (2003). The snow cover on lakes of the Arctic Coastal Plain of Alaska, USA. *Journal of Glaciology*, 49(166), 370-380.

Sturm, M., & Stuefer, S. (2013). Wind-blown flux rates derived from drifts at arctic snow fences. Journal of Glaciology, 59(213), 21-34.Tabler, R. D. (1975). Predicting profiles of snowdrifts in topographic catchment. In West. Snow Conf. Proc. (Vol. 43, pp. 87-97).

Tabler, R. (1986), Snow fence handbook, Release 1.0. Tabler & Associates, Laramie, WY.

Tabler, R. D. (2003). *Controlling blowing and drifting snow with snow fences and road design* (No. NCHRP Project 20-7 (147)).

Tominaga, Y., & Mochida, A. (1999). CFD prediction of flowfield and snowdrift around a building complex in a snowy region. *Journal of Wind Engineering and Industrial Aerodynamics*, *81*(1-3), 273-282.

Trujillo, E., Ramírez, J. A., & Elder, K. J. (2007). Topographic, meteorologic, and canopy controls on the scaling characteristics of the spatial distribution of snow depth fields. *Water Resources Research*, *43*(7).

Trujillo, E., Ramírez, J. A., & Elder, K. J. (2009). Scaling properties and spatial organization of snow depth fields in sub-alpine forest and alpine tundra. *Hydrological Processes: An International Journal*, *23*(11), 1575-1590.

Uematsu, T., Nakata, T., Takeuchi, K., Arisawa, Y., & Kaneda, Y. (1991). Three-dimensional numerical simulation of snowdrift. *Cold regions science and technology*, *20*(1), 65-73.

Van Leer, B. (1974). Towards the ultimate conservative difference scheme. ii. Monotonicity and conservation combined in a second-order scheme. Journal of computational physics, 14(4):361-370.

Van Leer, B. (1979). Towards the ultimate conservative difference scheme. v. a second-order sequel to godunov's method. Journal of computational Physics, 32(1):101-136.

Veitinger, J., Purves, R. S., & Sovilla, B. (2015). Potential slab avalanche release area identification from estimated winter terrain: a multi-scale, fuzzy logic approach. *Nat. Hazards Earth Syst. Sci. Discuss*, *3*, 6569-6614.

Vionnet, V., Martin, E., Masson, V., Guyomarc'h, G., Bouvet, F. N., Prokop, A., ... & Lac, C. (2014). Simulation of wind-induced snow transport and sublimation in alpine terrain using a fully coupled snowpack/atmosphere model.

Wang, W. H., Liao, H. L., & Li, M. S. (2014). Wind tunnel test on wind-induced roof snow distribution. *Journal of Building Structures*, *35*(5), 135-141.

Wangstrom, P. (1989). Collector snow fences in the artic. Northern Engineer, 21(1), 13-19.

Winstral, A., Elder, K., & Davis, R. E. (2002). Spatial snow modeling of wind-redistributed snow using terrain-based parameters. Journal of hydrometeorology, 3(5), 524-538.

Winstral, A., & Marks, D. (2002). Simulating wind fields and snow redistribution using terrain-based parameters to model snow accumulation and melt over a semi-arid mountain catchment. *Hydrological Processes*, *16*(18), 3585-3603.

Winstral, A., Marks, D., & Gurney, R. (2013). Simulating wind-affected snow accumulations at catchment to basin scales. Advances in Water Resources, 55, 64-79.

Yu, Z., Zhu, F., Cao, R., Chen, X., Zhao, L., & Zhao, S. (2019). Wind tunnel tests and CFD simulations for snow redistribution on 3D stepped flat roofs. *Wind and Structures*, *28*(1), 31-47.

Zhang, N., Kang, J. H., & Lee, S. J. (2010). Wind tunnel observation on the effect of a porous wind fence on shelter of saltating sand particles. *Geomorphology*, *120*(3-4), 224-232.

Zhou, X., Hu, J., & Gu, M. (2014). Wind tunnel test of snow loads on a stepped flat roof using different granular materials. *Natural hazards*, *74*(3), 1629-1648.

Zhou, X., Kang, L., Gu, M., Qiu, L., & Hu, J. (2016). Numerical simulation and wind tunnel test for redistribution of snow on a flat roof. *Journal of Wind Engineering and Industrial Aerodynamics*, *153*, 92-105.

## Captions of Figures

Figure 1. Verification of the numerical algorithm by the analytical (exact) solution (Equation 11) of the LPD equation for typical solid (upper) and perforated (lower) snow fence cases.

Figure 2. Schematic of the proposed model configuration using an equivalent solid snow fence and its area of influence.

Figure 3. Model-simulated snowdrift profiles (area graph) and the corresponding observed synthesized snow distributions (dots) (Tabler, 2003). Wind direction is from left to right.

Figure 4. Model domains for SMOOTH model performance with and without snow fences in Southeast Wyoming. The Malody and Honey Tree areas were utilized for simulations with snow fences. Dale Creek (relatively open with some riparian vegetation) and Blair Wallis (partially forested open area) were selected for simulations without snow fences.

Figure 5. LiDAR-observed and model-simulated snowdrifts in Malody (calibration) and Honey Tree (validation) snow fence areas along Interstate 80, Southeast Wyoming. The wind rose used the data from the closest Road Weather Information System (RWIS) site (KVDW).

Figure 6. LiDAR-observed and model-simulated snowdrifts in Dale Creek (calibration) and Blair Wallis (validation) in the open and partially forested areas without snow fences at Southeast Wyoming.

Figure 7. Snowdrift stratigraphy imaged with GPR (solid lines) and the model-simulated snow depths (dashed lines) along the line perpendicular to the lakeshore cliff in Inigok, North Slope, Alaska.

Figure 8. Measured and model-simulated snow distributions in CALM, east of Utqiagvik, Alaska. The upper panel shows the elevation and snow surface profiles along the line A-A' in the lower right panel. The prevailing wind is typically from the east (right) in this area.

Figure 9. Fractional contributions of the particle motion parameters (a = diffusion, b = advection, and c = erosion coefficient) to the snowdrifts in the applications in Wyoming and Alaska. (a)-(d) one-dimensional synthesized snow profiles for various snow fence types; (e) two-dimensional snow distribution around snow fence on the natural terrain; (f) snow distribution on the open terrain including incised channel gully; (g) snow surface profile across the lakeshore cliff in Inigok; and (h) snow distribution on the open arctic terrain in CALM.

## Tables

Table 1. Model parameters and performance root mean square difference (RMSD) for the SMOOTH model application shown in Figure 7.

| | a | b | c | f | RMSD (m) | Lapse time (hour) |
|---|---|---|---|---|---|---|
| Surface | -0.009 | 0.0008 | 0 | 0 | 0.217 | 549 |
| rflex1 | -0.012 | 0.0104 | 0.0002 | -0.0007 | 0.057 | 57 |
| rflex2 | -0.0055 | 0.0029 | -0.00021 | -0.0006 | 0.14 | 112 |
| rflex3 | -0.0015 | 0.0059 | -0.0003 | -0.0009 | 0.093 | 83 |
| rfex4 | -0.0005 | 0.0014 | -0.00004 | -0.0003 | 0.061 | 321 |

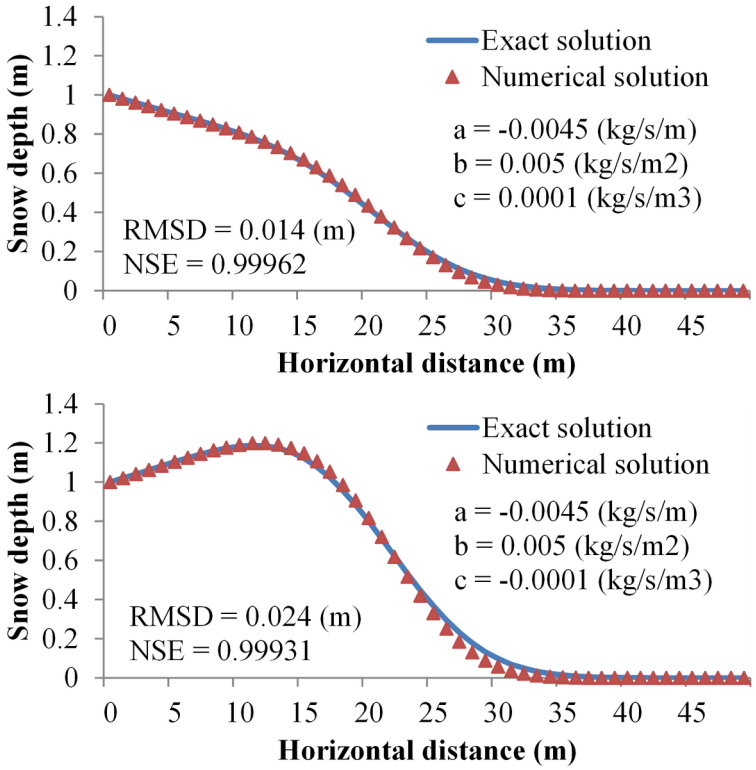


HYP_14468_Fig1.tif

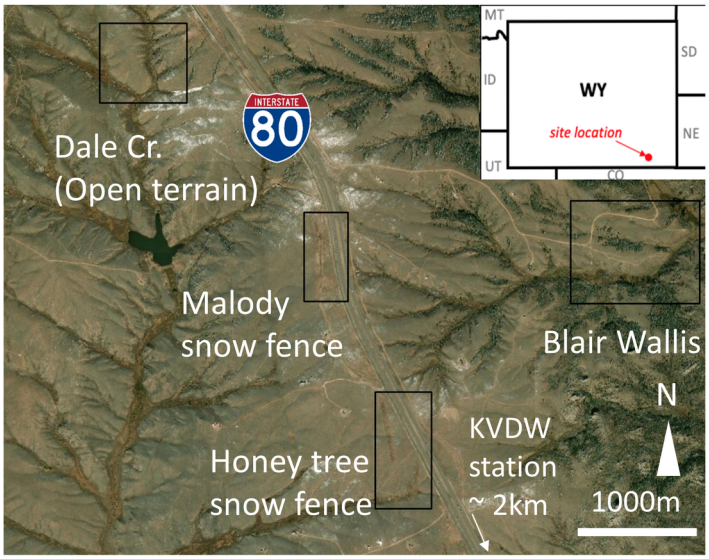


HYP_14468_Fig4_20210923.tif

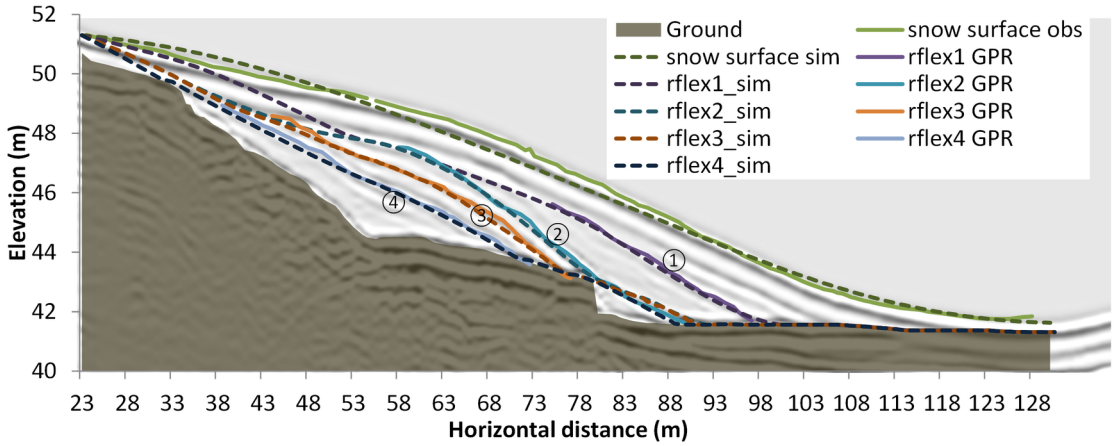


HYP_14468_Fig7_20210923.tif

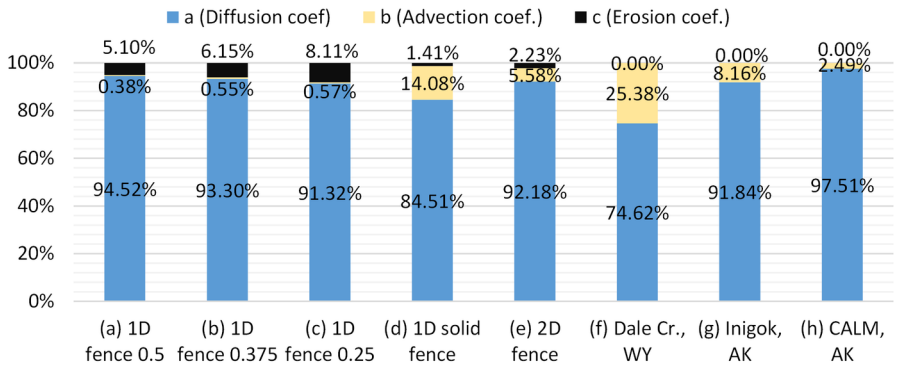


HYP_14468_Fig9_20210923.tif

**Spatial Snowdrift Modeling for an Open Natural Terrain using a Physically-based Linear Particle Distribution Equation**

**Noriaki Ohara*, Siwei He, Andrew D. Parsekian, Benjamin M. Jones, Rodrigo C. Rangel, Ian O. Nichols, and Kenneth M. Hinkel**

The numerical model (SMOOTH model) based on the Linear Particle Distribution (LPD) equation is useful to separate the snow particle motion effects: dispersion, advection, and erosion. The model can reproduce the observed spatial snowdrifts with snow fences and abrupt terrain features.

Linear Particle Distribution (LPD) equation =Diffusion + Advection + Erosion

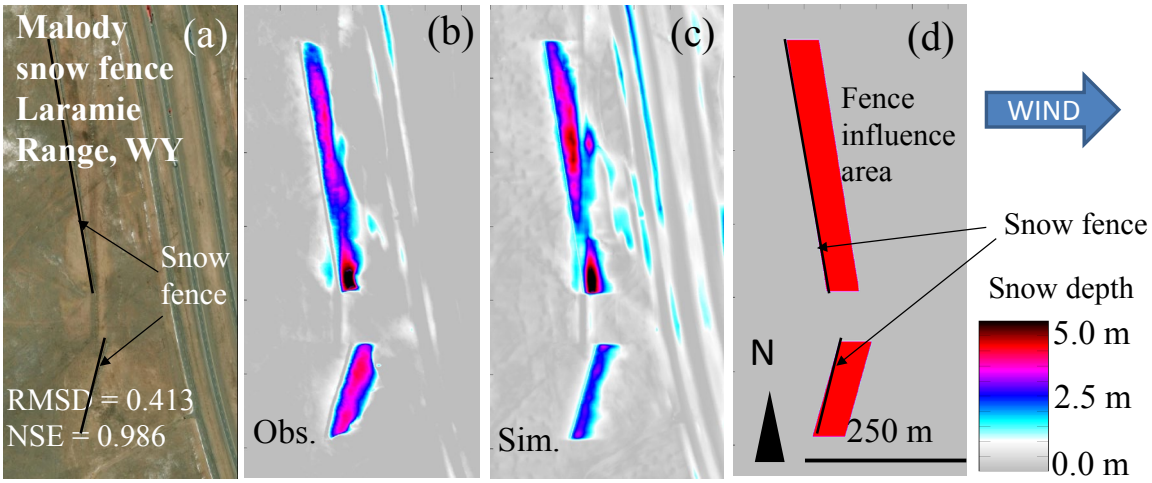

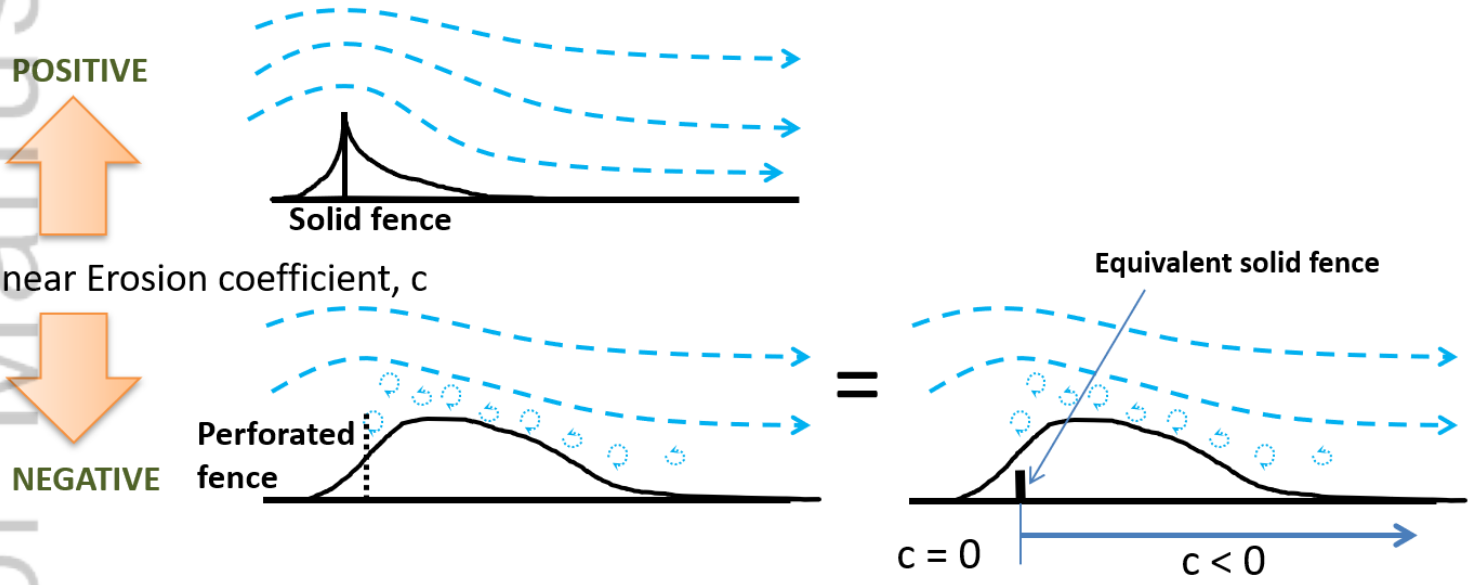


HYP_14468_Picture2.tif

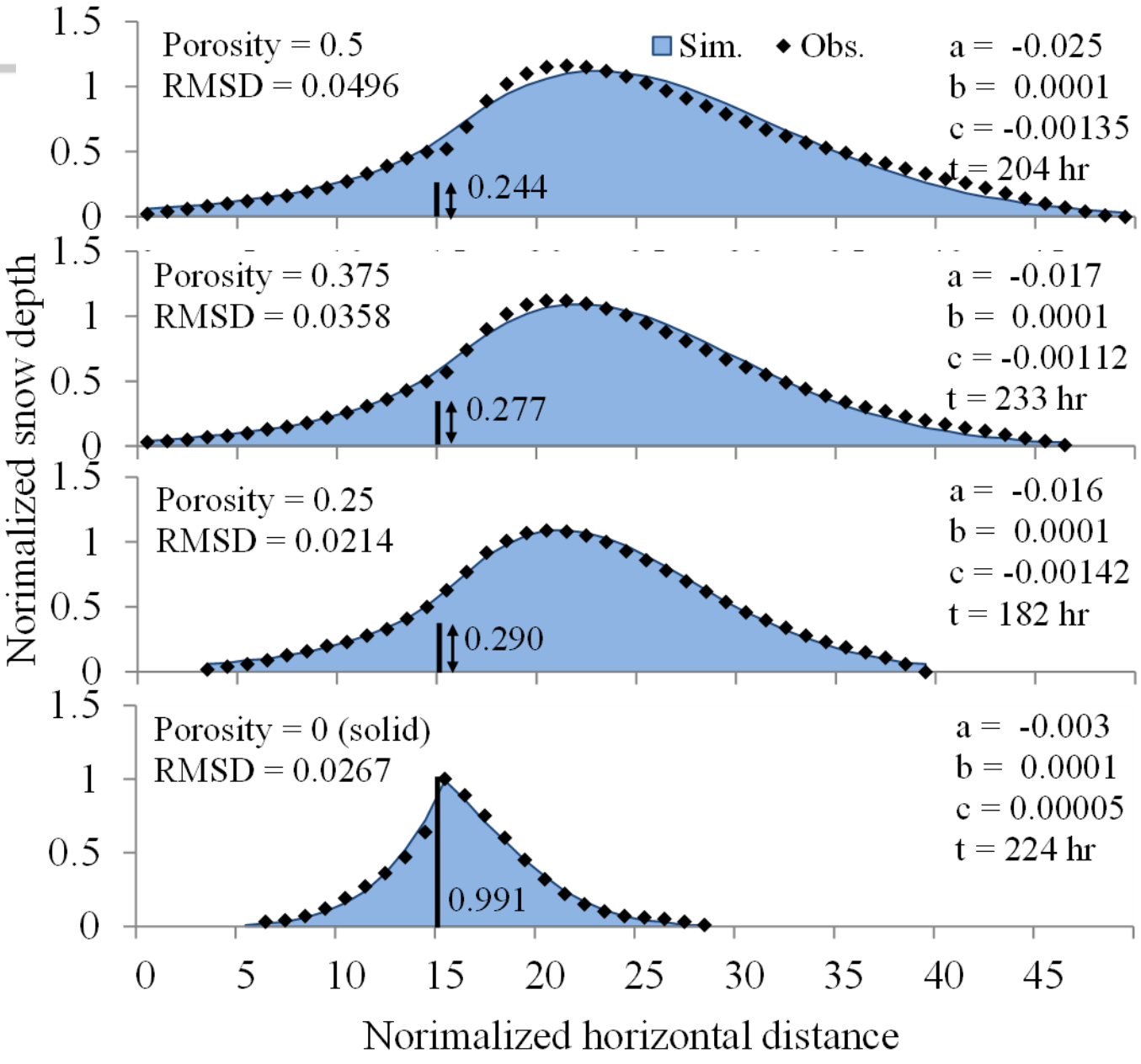


HYP_14468_Picture3.tif

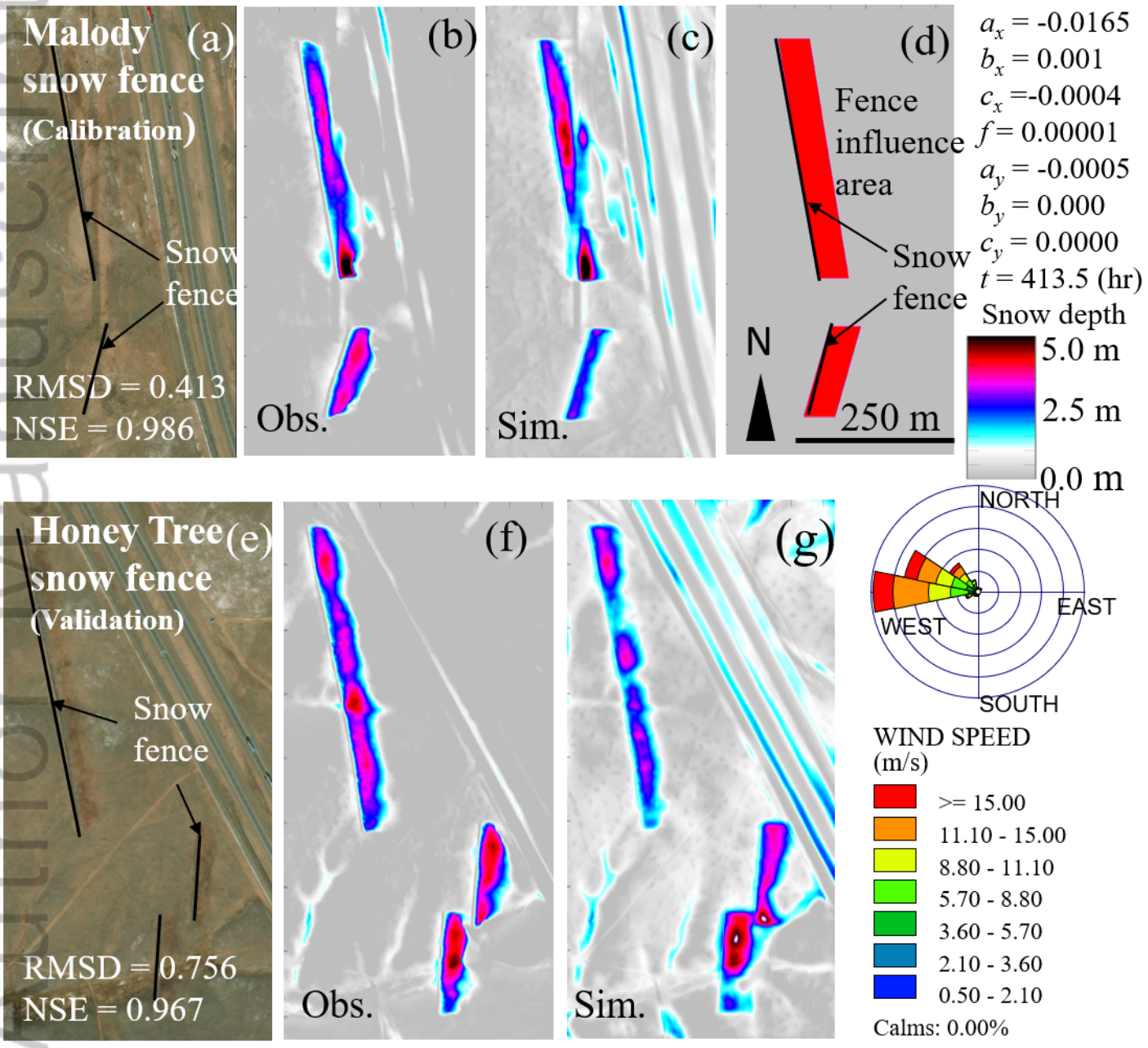


HYP_14468_Picture5.tif

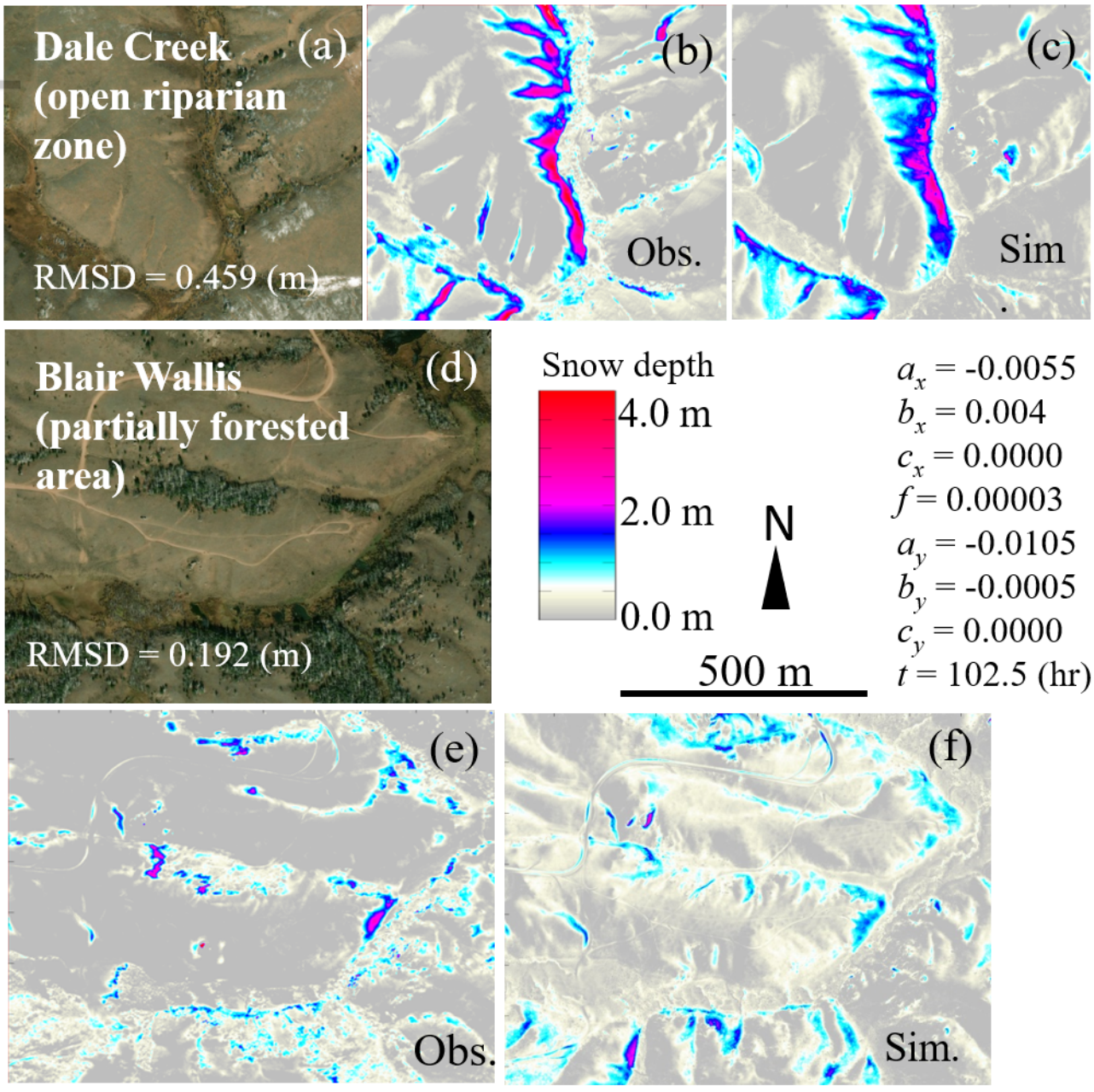


HYP_14468_Picture6.tif

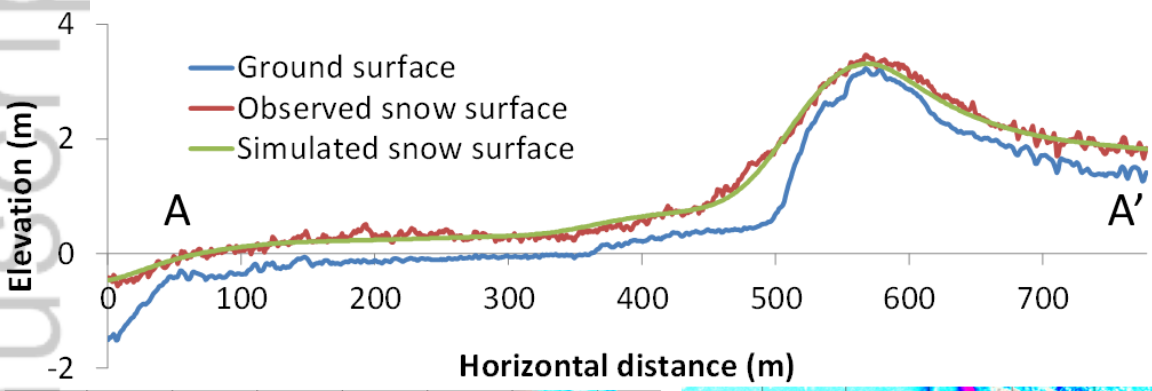


$a_x$ = -0.0365
$b_x$ = -0.001
$c_x$ = 0.0000
$f$ = 0.00003
$a_y$ = -0.014
$b_y$ = 0.000
$c_y$ = 0.0000
$t$ = 1064 (hr)

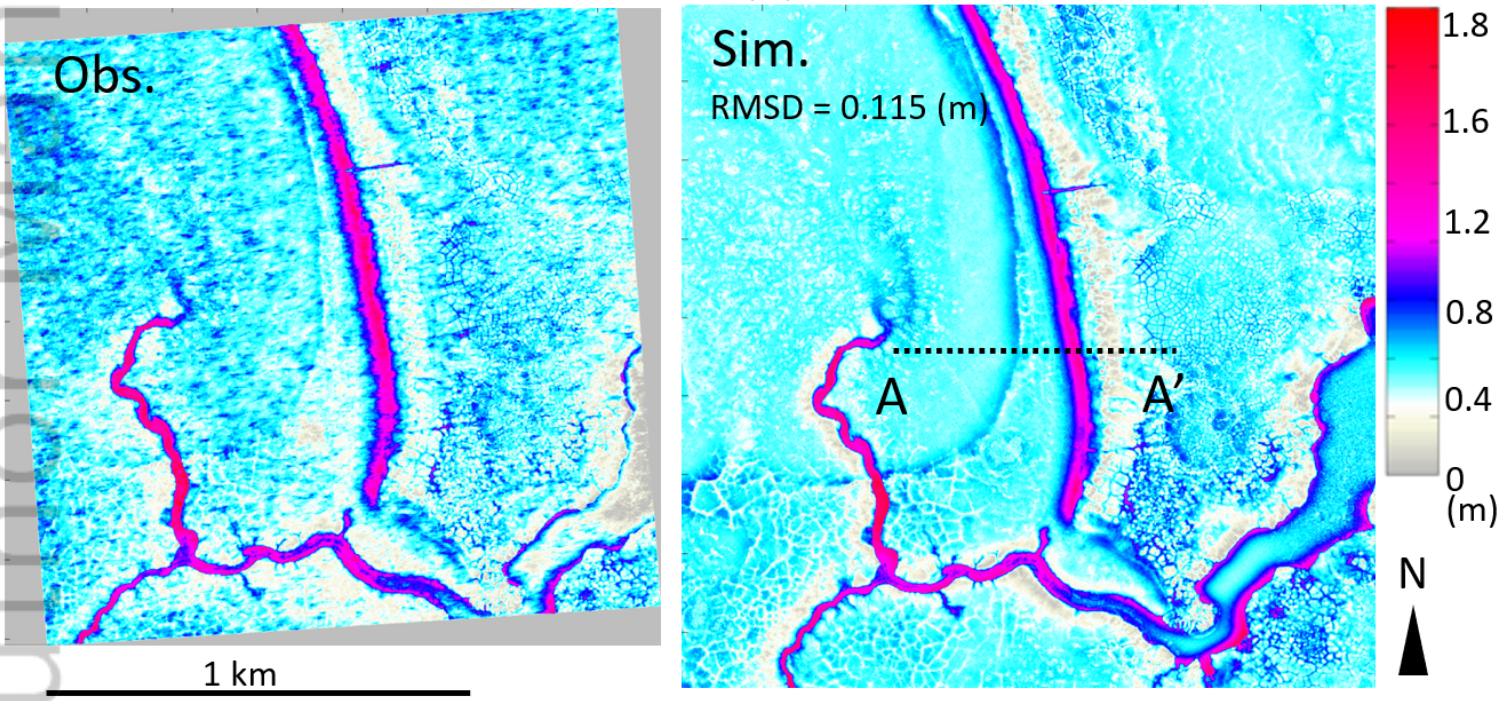


HYP_14468_Picture8.tif